THE ASTROPHYSICAL JOURNAL SUPPLEMENT SERIES, 126:63–78, 2000 January

VISIBLE AND NEAR-INFRARED SPECTROSCOPY OF SEYFERT 1 AND NARROW-LINE SEYFERT 1 GALAXIES[1]

ALBERTO RODRÍGUEZ-ARDILA[2,3,4] AND MIRIANI G. PASTORIZA
Departamento de Astronomia–UFRGS. CP 15051, Porto Alegre, RS, Brazil

AND

CARLOS J. DONZELLI[2]
IATE, Observatorio Astronómico, Universidad Nacional de Córdoba Laprida 854, 5000, Córdoba, Argentina
Received 1999 May 27; accepted 1999 August 24

ABSTRACT

This paper studies the continuum and emission-line properties of a sample composed of 16 normal Seyfert 1 and seven narrow-line Seyfert 1 (NLS1) galaxies using optical and near-IR CCD spectroscopy. The continuum emission of the galaxies can be described in terms of a combination of stellar population, a nonstellar continuum of power-law form, and Fe II emission. A significative difference in the optical spectral index between NLS1's and normal Seyfert 1's is observed; the latter is steeper. Most NLS1's show Fe II/Hβ ratios larger than those observed in the other Seyfert 1's. In the *IRAS* band, both groups of galaxies have very similar properties. We have searched for the presence of optically thin gas in the broad-line region (BLR) of the galaxies by comparing the broad O I λ8446 and Hα emission-line profiles. Our analysis show that in the NLS1's, both profiles are similar in shape and width. This result contradicts the hypothesis of thin gas emission in the high-velocity part of the BLR to explain the "narrowness" of broad optical permitted lines in these objects. Evidence of narrow O I λ8446 emission is found in six galaxies of our sample, implying that this line is not restricted to a pure BLR phenomenon. In the narrow-line region, we find similar luminosities in the permitted and high-ionization lines of NLS1's and normal Seyfert 1's. However, low-ionization lines such as [O I] λ6300, [O II] λ3727, and [S II] $\lambda\lambda$6717, 6731 are intrinsically less luminous in NLS1's. Physical properties derived from density- and temperature-sensitive line ratios suggest that the [O II] and [S II] emitting zones are overlapping in normal Seyfert 1's and separated in NLS1's.

Subject headings: galaxies: nuclei — galaxies: Seyfert — X-rays: galaxies

1. INTRODUCTION

Nuclear emission-line spectra of Seyfert 1 (Sy1) galaxies are mainly characterized by the presence of broad permitted lines with typical full width at half-maximum (FWHM) between 4000 and 10,000 km s^{-1} and narrow permitted and forbidden lines with FWHM in the interval 300–900 km s^{-1}. The former lines originate in the innermost central region (<1 pc in size), the so-called broad line region (BLR), while the later are formed in the outer, more extended ($\sim$100 pc), narrow-line region (NLR).

In addition, there is a peculiar group of AGNs known as narrow-line Seyfert 1 (hereafter NLS1) galaxies, located at the lower end of the broad line width distribution, with permitted lines having a FWHM in the interval 1000–2000 km s^{-1}. In most other properties, NLS1's are similar to "normal" Seyfert 1's except in the soft X-ray band, where they have generally much steeper continuum slopes and present in a few cases rapid variability (Boller, Brandt, & Fink 1996). In the optical, their Fe II emission is among the strongest detected in AGNs.

The narrowness of the broad permitted lines in NLS1's is usually interpreted as a combined effect between a particular geometry of the emitting clouds and an orientation effect. If the clouds are arranged in a planar geometry with its rotating axis almost parallel to the line of sight, the observed radial velocity distribution would be smaller (pole-on model; Boller et al. 1996).

However, Rodríguez-Pascual, Mass-Hesse, & Santos-Lléo (1997) report the detection in NLS1 galaxies of broad components with FWHM around 5000 km s^{-1} in high-ionization UV permitted lines such as Lyα, He II λ1640, and C IV λ1550. This result indicates that gas moving at velocities comparable to those found in typical Sy1 galaxies does indeed exist in NLS1's. The absence of broad lines (that is, lines with FWHM larger than 3000 km s^{-1}) seems then to be restricted to the optical permitted lines.

While most efforts have been devoted to explaining the narrowness of broad permitted lines and the X-ray properties in NLS1's, very little has been said regarding the properties of the NLR in these objects. It is known that NLS1's usually have [O III] λ5007/Hβ < 3, much smaller than that in Seyfert 2 galaxies, and strong forbidden lines of highly ionized atoms. Except for a few spectral studies (Osterbrock & Pogge 1985; Goodrich 1989; Stephens 1989) no quantitative analysis involving NLR emission-line ratios and a comparison to those of "normal" Sy1's have been done so far. For this reason, we have carried out a spectroscopic study of 23 galaxies, seven of which are classified as NLS1's and the remaining ones as "normal" Sy1's.

It is important to note that the adjective "normal" is used only as a semantic discriminator, and it implies Seyfert 1 galaxies with FWHM larger than 3000 km s^{-1} in the permitted lines. We are aware both of the wide heterogeneity of Sy1's as well as the fact that the properties of

[1] Based on observations made at CASLEO. Complejo Astronómico El Leoncito (CASLEO) is operated under agreement between the Consejo Nacional de Investigaciones Científicas y técnicas de la República Argentina and the National Universities of La Plata, Córdoba and San Juán.

[2] Visiting Astronomer at CASLEO Observatory

[3] CNPq Fellow.

[4] E-mail:alberto@if.ufrgs.br.

NLS1's and normal Sy1's probably form a continuous distribution.

The present paper is organized as follows. In § 2 we give a description of the observations and reduction procedure. Section 3 discusses the properties of the optical and IR continuum of the sample. The measurement and analysis of the line fluxes and line profiles is carried out in § 4, and the study of the NLR of the galaxies is given in § 5. Our conclusions are in § 6. A value of the Hubble constant of $H_0 = 75$ km s^{-1} Mpc^{-1} has been assumed throughout.

2. OBSERVATIONS AND DATA REDUCTION

The sample of Sy1 galaxies chosen for this study was taken primarily from the Calán-Tololo Survey (Maza et al. 1989, 1992, 1994) for two reasons. First, it is mainly composed of objects with little or no information available in the literature since they were classified as Sy1's recently. In this sense, they form an unexplored and valuable set of data, with some of the galaxies displaying very interesting spectral features. Second, the FWHM of the permitted emission lines forms a natural continuous sequence varying from 3000 up to 7000 km s^{-1}, allowing the search for differences between emission-line properties of the NLR in NLS1 and Sy1 galaxies. The targets were selected from a list of more than 100 candidates. The only constraints applied were that the visual magnitude was brighter than 17 (to avoid long exposure times) and that the object had not been extensively studied in the optical region.

The NLS1 sample (Mrk 1239, 1H 1934−063, CTS R12.02, CTS J04.08, CTS J13.12, CTS J03.19, and CTS H34.06) is composed of objects that are typical representative of its class. The first four galaxies have available data in the *IRAS* bands and soft X-ray region. CTS J04.08, CTS J13.12, CTS J03.19, and CTS H34.06 were classified as NLS1 by us based on the appearance of their optical spectrum. Except for CTS J04.08, they have no published data in the literature.

The fundamental properties of the galaxies, obtained from the NED[5] database, are listed in Table 1.

Long-slit spectra were obtained with the 2.15 m telescope of the Complejo Astronómico El Leoncito (CASLEO) during many observing runs using a TEK 1024 × 1024 CCD detector and a REOSC spectrograph. A log of the observations is given in Table 2. Two gratings of 300 line mm^{-1} with blaze angles near 5500 and 8000 Å were used in order to cover the spectral interval 3700–9500 Å. The spatial scale of this setup is 0.″95 pixel^{-1}, with a resolution of 4 Å pixel^{-1}. In all cases it was employed a slit width of 2.″5 oriented in the east-west direction. The galaxies and standard stars were observed near the zenith (air masses < 1.2). The typical length of the spectral extraction window for the objects was between the four and eight innermost central pixels, depending on the seeing conditions during the observations. Atmospheric absorption bands were removed by dividing the object spectra by a smoothed and spline-fitted (but retaining the atmospheric bands) flux curve derived from a standard star spectrum observed at similar zenith distance to that of the object.

Data reduction was performed with standard IRAF[6] tasks. The spectra were calibrated in wavelength using comparison lamps of He-Ne-Ar, taken at the beginning and end of each object exposure. In all cases, the rms values of the wavelength calibration were less than 0.1 Å.

[5] The NASA/IPAC Extragalactic Database (NED) is operated by the Jet Propulsion Laboratory, California Institute of Technology, under contract with the National Aeronautics and Space Administration.

[6] IRAF is distributed by NOAO, which is operated by AURA Inc., under contract to the NSF.

TABLE 1

FUNDAMENTAL PROPERTIES OF THE GALAXY SAMPLE

Galaxy (1)	Type (2)	m_v (3)	V_r (km s^{-1}) (4)	$E(B-V)_G$ (5)	R (kpc) (6)	Morphology (7)
CTS C16.16	Sy1	17.0	22864±500	0.0	4.9	...
MCG −5-13-17.....	Sy1	12.5	3825±150	0.0	0.8	S0/a
CTS H34.03	Sy1	15.8	28978±300[a]	0.08	6.2	...
CTS B31.01.....	Sy1	17.0	10154±180	0.02	3.2	...
CTS H34.06	NLS1	16.2	9547±100[a]	0.05	2.0	...
Fairall 1146.....	Sy1	16.1	9521±100	0.15	3.1	Sb
Mrk 1239	NLS1	13.3	6033±70	0.03	0.6	E–S0
CTS J03.19	NLS1	15.7	15948±180[a]	0.05	3.4	...
CTS J04.08	NLS1	15.6	11997±80	0.06	7.7	...
CTS M02.30.....	Sy1	16.2	20612±250[a]	0.05	4.4	SB
CTS J07.02	Sy1	14.6	9816±90	0.02	1.1	Irr
CTS J10.09	Sy1	16.2	6906±20[a]	0.03	1.5	...
CTS R12.15	Sy1	14.5	4269±100	0.0	0.5	Sa
CTS R12.02	NLS1	14.3	4104±50	0.02	1.6	Sa
CTS J13.12	NLS1	17.4	3590±50	0.06	0.8	...
CTS J14.05	Sy1	15.2	10388±90[a]	0.06	3.4	...
CTS J15.22	Sy1	16.2	33794±800	0.08	7.3	N
CTS M17.17.....	Sy1	14.4	3188±90	0.10	1.0	(R)SB(1)0$^+$
CTS G03.04	Sy1	15.2	11657±300	0.03	2.5	(R)SB0/a
1H 1934−063	NLS1	14.1	3044±80	0.18	0.7	E
1H 2107−097	Sy1	14.3	7952±70	0.08	1.7	...
CTS A08.12	Sy1	15.5	8780±100	0.03	1.9	...
CTS F10.01.....	Sy1	15.6	23500±150	0.0	5.0	...

[a] First determination of radial velocity.

TABLE 2

LOG OF OBSERVATIONS

Object	UT Date	λ_c (Å)	Grid	Exposure Time (minutes)
CTS C16.16	1996 Aug 10	6900	H	20
	1996 Aug 11	6300	H	20
	1996 Aug 12	7000	L	45
	1996 Aug 13	7000	L	45
	1997 Aug 30	5300	L	60
	1997 Aug 30	5300	L	30
MCG −5-13-17.....	1996 Mar 22	5500	L	30
	1999 Mar 18	8000	L	30
	1999 Mar 19	5300	L	30
CTS H34.03	1996 Mar 21	5500	L	45
	1997 Apr 06	8000	L	45
	1997 Apr 07	5300	L	45
CTS B31.01.....	1996 Mar 23	5500	L	15
	1999 Mar 17	8000	L	20
	1999 Mar 19	5300	L	40
CTS H34.06	1996 Mar 23	6200	L	15
	1997 Apr 05	8000	L	45
	1999 Mar 19	5300	L	20
Fairall 1146.....	1996 Mar 22	5500	L	40
	1997 Apr 05	8000	L	40
Mrk 1239	1996 Mar 21	5500	L	30
	1997 Apr 05	8000	L	35
CTS J03.19	1996 Mar 22	5500	L	15
	1997 Apr 06	8000	L	45
	1997 Apr 08	5300	L	30
	1999 Mar 18	5300	L	30
CTS J04.08	1996 Mar 22	5500	L	15
	1997 Apr 08	5300	L	30
	1999 Mar 17	8000	L	20
CTS M02.30.....	1996 Mar 23	6200	L	15
	1997 Apr 07	8000	L	45
	1997 Apr 08	5300	L	45
CTS J07.02	1996 Mar 21	5500	L	30
	1997 Apr 07	8000	L	45
CTS J10.09	1997 Apr 08	5300	L	30
	1999 Mar 17	8000	L	20
CTS R12.15	1996 Mar 21	5500	L	30
	1997 Apr 06	8000	L	45
CTS R12.02	1999 Mar 17	8000	L	20
	1999 Mar 19	5300	L	20
CTS J13.12	1997 Apr 07	8000	L	45
	1997 Apr 08	5300	L	30
CTS J14.05	1996 Mar 22	5500	L	30
	1997 Apr 06	8000	L	45
	1997 Apr 08	5300	L	30
CTS J15.22	1996 Mar 23	6200	L	45
	1997 Apr 07	8000	L	45
CTS M17.17.....	1996 Mar 21	5500	L	45
	1997 Apr 06	8000	L	45
	1997 Apr 08	5300	L	30
CTS G03.04	1997 Aug 29	8300	L	60
	1997 Aug 30	5300	L	30
1H 1934−063	1996 Aug 10	6900	H	20
	1997 Aug 29	8300	L	60
	1997 Aug 30	5300	L	60
1H 2107−097	1996 Aug 11	6900	H	15
	1996 Aug 13	7000	L	30
	1996 Aug 14	5550	L	45
	1997 Aug 29	8300	L	45
	1997 Aug 30	5300	L	60
CTS A08.12	1997 Aug 29	8300	L	60
	1997 Aug 30	5300	L	60
CTS F10.01.....	1997 Aug 29	8300	L	60
	1997 Aug 30	5300	L	60

Flux calibration was carried out using observations of standard stars of Stone & Baldwin (1983) taken at the beginning, middle, and end of each night. In order to link up the intensity scale in the optical and near-IR in each galaxy, we used the strongest common lines that could be identified and measured in the overlapping regions of the spectra. Care was taking in obtaining both spectra on consecutive nights in order to obtain a good match between the optical and near-IR regions.

The spectra were corrected for redshift derived from the strongest narrow emission lines observed. Usually [O III] λ5007, Hα, Hβ, [O I] λ6300, and [S II] $\lambda\lambda$6717, 6731 were used for this purpose. The results are in very good agreement to those published in the literature. The radial velocity measured for each galaxy is listed in column (4) of Table 1. Galaxies marked with footnote a have no previous measurement of V_r. The size of the observed region (in kpc) is listed in column (6).

Figure 1 presents the spectra of the 23 galaxies observed, already corrected for redshift and in increasing order of right ascension. NLS1's are identified from the remaining normal Sy1 galaxies.

3. CONTINUUM DECOMPOSITION

Before measuring the flux of the emission lines, it is necessary to determine and subtract the components of the observed continuum given that it affects the determination of the true level of the base of the lines as well as the form and width of the emission-line profiles. Such is the case of the Hβ+[O III] $\lambda\lambda$4959, 5007 blend, which is affected by the presence of the Fe II emission located under and at both sides of these lines, or the Hγ+[O III] λ4363 lines, whose flux can be overestimated if the stellar continuum is strong.

We first searched for signatures of underlying stellar population from the host galaxy, whose contribution must be determined and subtracted in order to get a pure nuclear continuum. This can be carried out by measuring the equivalent width of absorption features such as Ca II K λ3933, CN G λ4301 and Mg+MgH λ5175 following the method and templates described in Bica (1988). In CTS M17.17, CTS R12.15 and MCG −5-13-17, it was found that 60%, 70%, and 44%, respectively, of the continuum at 5870 Å was of stellar origin. The template that best reproduced the stellar populations in these galaxies was the S6, which is representative of stellar population with important contribution ($\sim$25%) of young stars with age $< 5 \times 10^7$ yr.

In the remaining AGNs, the absorption bands were diluted by the strong nuclear continuum. We determined that the contribution of the stellar light to the observed continuum at 5870 Å in these objects was no higher that 10%. No effort was made to subtract the stellar population from them.

A nonstellar continuum of power-law form was also observed in most spectra. The task *nfit1d* of the STSDAS package of IRAF was used to fit a function of the type $F_\lambda = K * (\lambda/\lambda_{\rm ref})^\alpha$ to the observed continuum. In the above relation, K (the amplitude of the power law at the reference wavelength $\lambda_{\rm ref}$) and the spectral index α are parameters to be determined from the fit. $\lambda_{\rm ref}$ was set to 4780 Å. In order to obtain a good fit, regions free of emission lines such as 4780 Å, 5400 Å, 5900 Å, redward of Hα, and 7500 Å were chosen as reference points. Column (9) of Table 5 lists the values of α found from the fit. A clear difference between the power-law index in NLS1 and

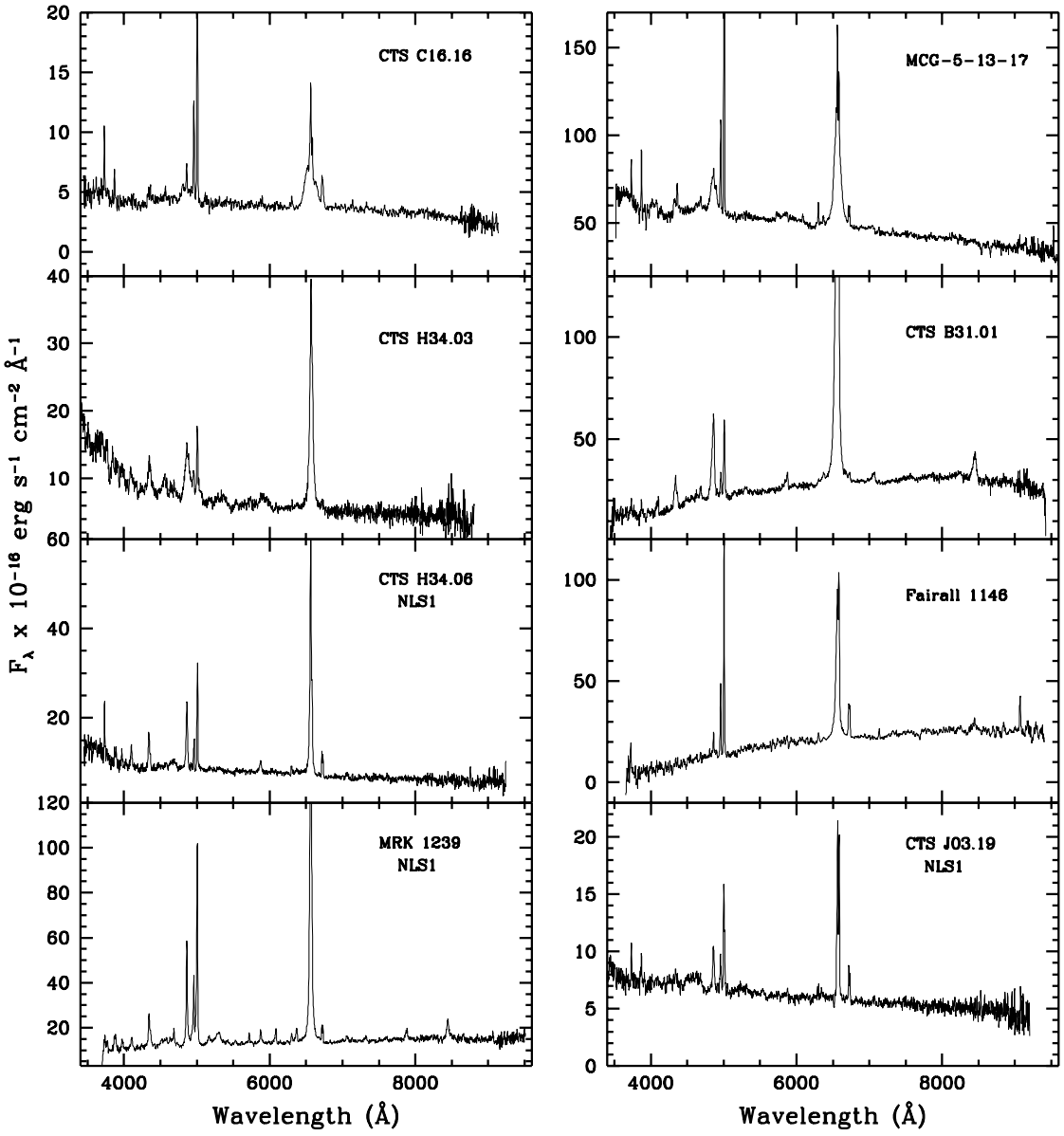

FIG. 1.—Spectra of the observed galaxies, in increasing order of right ascension, already corrected for redshift. Narrow-line Seyfert 1 galaxies are identified from the normal Sy1 galaxies.

normal Seyfert 1 galaxies is observed, with normal Sy1's usually presenting steeper slopes. The average value of α is -0.59 for NLS1's, -0.90 for normal Sy1's, and -0.79 for the whole sample. This result contrasts with what is reported in the X-ray spectral region, where NLS1's usually have steeper X-ray continuum slopes than normal Sy1's. However, we have to treat the above figures with caution owing to the small number of objects in our sample.

Some of the galaxies also show a pseudocontinuum created by the blending of several Fe II multiplets. It is evident as two bumps centered at 4570 and 5250 Å and is particularly strong in NLS1's, where Fe II λ4570/Hβ is usually larger than 0.8 (Boller et al. 1996). As a comparison, the median value of the distribution of this ratio in the AGN sample of Joly (1991) is about 0.53.

In order to quantify and subtract this component, we followed the procedure employed by Rodríguez-Ardila, Pastoriza, & Maza (1998), consisting of estimating the strength of the Fe II lines in the optical region using the spectrum of I Zw 1 as a template. This NLS1 galaxy is widely known for having a very strong Fe II spectrum, which can be isolated and then scaled up to match the observed Fe II emission.

The Fe II λ4570/Hβ ratio found in each object is listed in column (8) of Table 5. Average values of this ratio are 0.92 and 0.53 for NLS1's and normal Sy1's, respectively. These numbers are in accord with the values reported in the literature and clearly reflect the fact that NLS1's are stronger Fe II emitters. In terms of frequency, all of our NLS1 galaxies show Fe II emission, in contrast to the 44% observed in normal Sy1's.

3.1. *Infrared Properties of the Sample*

We have used the 12 μm, 25 μm, 60 μm, and 100 μm *IRAS* fluxes of the galaxies, listed in Table 3, to analyze the nature of the infrared emission in these objects. In particu-

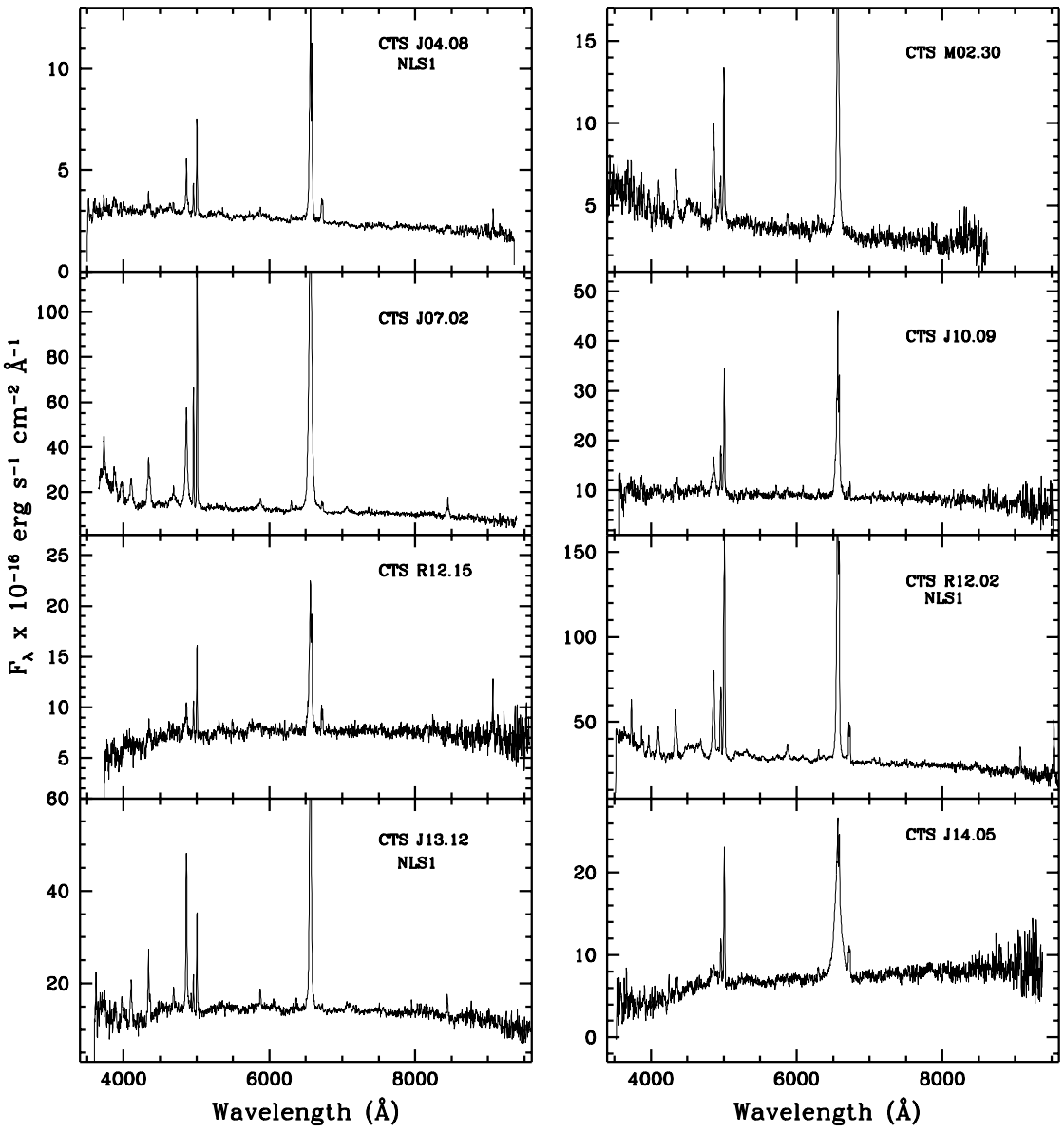

FIG. 1.—*Continued*

lar, we wish to determine if the observed fluxes result from dust directly heated by the active galactic nucleus (warm dust), from the host galaxy (cool dust), or a combination of these two processes.

For this purpose we have calculated the $\alpha(25, 12)$ and $\alpha(100, 60)$ color indices using the expressions given in Bonatto & Pastoriza (1997, hereafter BP97). The results are listed in columns (7) and (8) of Table 3. These colors are intended to estimate the effect of a cool dust component on Seyfert pure color indices, taking into account the fact that in normal spiral galaxies the observed 60 μm and 100 μm fluxes can be almost entirely accounted for by a combination of relatively cool (20–25 K) dust heated by the interstellar radiation field and warmer dust heated by O and B stars (Walterbos & Greenwalt 1996).

As a first result, NLS1's and normal Sy1's have very similar behavior. They share the same loci of points as the Seyfert 1 galaxies of BP97 (see Fig. 4 of BP97 and our values of color indices of Table 3). This indicates that the IR colors of our sample can be explained as a result of dust heated directly by the AGN source with some fraction of emission from cool dust ($0.2 \leq \beta \leq 0.6$) with evaporation temperature of $T_{ev} = 1500$ K. The only exception is 1H 2107−097, which shows $\alpha(100, 60) = -3.9$, indicating that it is redder than the remaining objects, with a strong contribution of cool dust at 12 μm ($\sim$10%).

Regarding to the total infrared luminosity, we also found no significative differences between the values of L_{IR} displayed by both groups, as can be seen in the last column of Table 3.

4. THE EMISSION-LINE SPECTRUM AND EMISSION-LINE PROPERTIES OF THE GALAXIES

The integrated flux of the emission lines were measured assuming that they were well represented by Gaussian profiles. The LINER routine, a χ^2 minimization algorithm that fits as many as eight Gaussians to a line profile, was used for this purpose. For heavily blended lines such as Hα+[N II] or Hβ+[O III], theoretical line ratios and known fixed wavelength separations between forbidden lines were

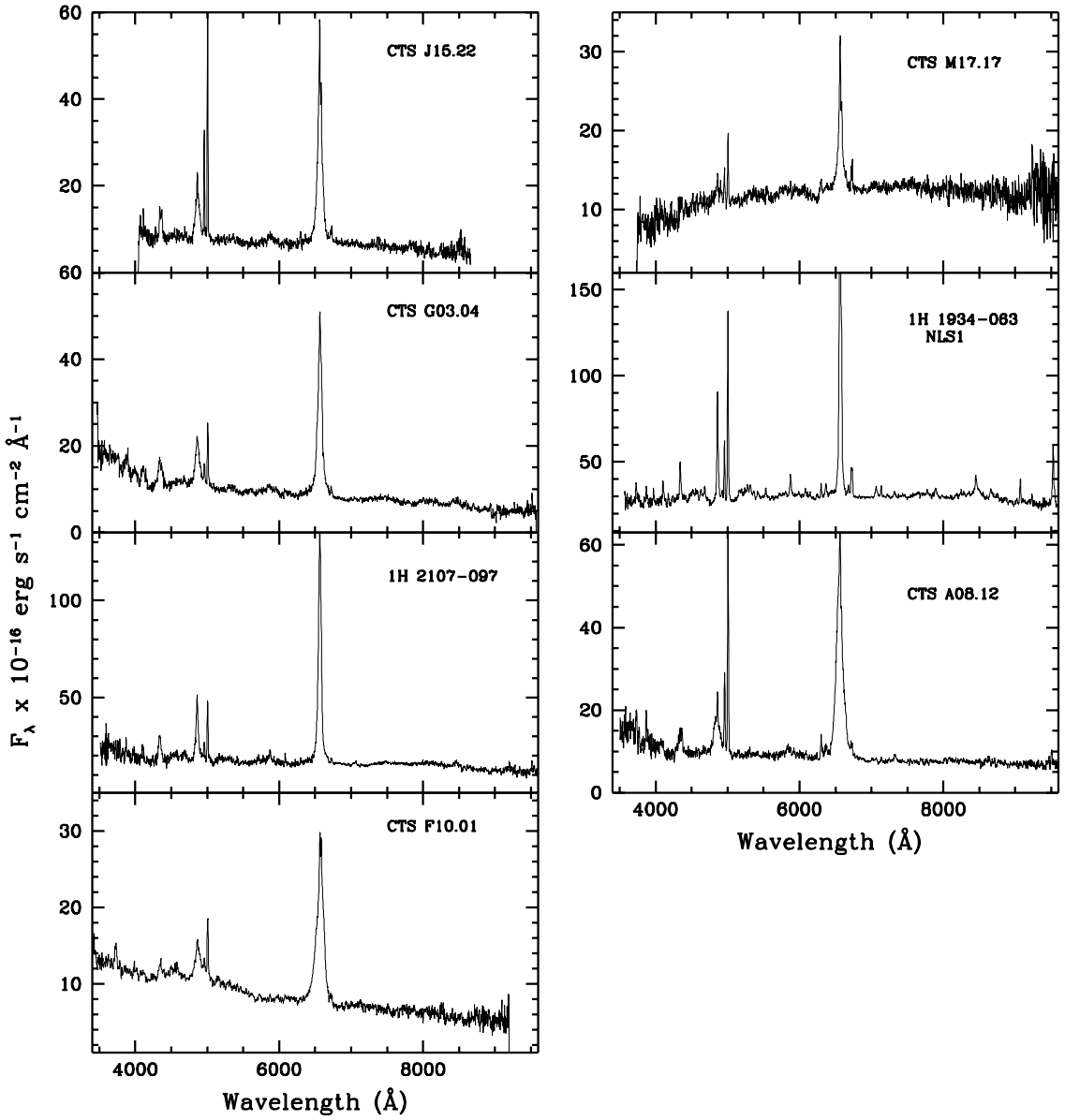

FIG. 1.—*Continued*

employed to constrain the fit. In some cases it was necessary to fit up to three Gaussians to the permitted lines in order to match satisfactorily the synthetically calculated profile to the observed one.

Figure 2 shows an example of the deblending process applied to the Hα+[N II] $\lambda\lambda$6548, 6584 lines of the NLS1 galaxies CTS J04.08 (*a*) and Mrk 1239 (*b*) and the normal Seyfert 1 galaxies CTS J15.22 (*c*) and CTS J04.08 (*d*). The wavelength axis is in velocity space, with $V_e = 0$ representing the rest wavelength of Hα = 6563 Å. Although not evident at first sight, it can be seen that in the former two galaxies there is a broad component with FWHM near 2000 km s^{-1}, not as broad as those clearly observed in the normal Seyfert 1's. Note also that in the NLS1's, most of the core of Hα is dominated by a component of FWHM very similar to that of the forbidden lines [N II] $\lambda\lambda$6548, 6584. A comparison of the width of the narrow lines in the four panels allows us to associate the narrow Hα line in NLS1's with emission from the NLR. Figure 2 also shows that it is possible to carry out a clean separation between the "broad" and narrow components in NLS1's, provided the signal-to-noise ratio (S/N) of the spectra is good, as it is the case.

The χ^2 residuals of the Gaussian fits were $\sim$1% for strong lines and $\sim$5%–10% for weaker ones. Lines of ions such as [Fe X] λ6371, [Fe VII] λ6085, and most near-IR lines have rms values somewhat larger, and their fluxes are accurate only to within 10%–30%. Tables 4 and 5 give the measured narrow- and broad-line fluxes, respectively. Note that [O II] λ3727 = (λ3726+λ3729) and [O II] λ7325 = (λ7320+λ7330).

The last column of Table 4 lists the $E(B-V)$ determined from the Balmer decrement Hα/Hβ assuming an intrinsic ratio of 3.1. In this calculation, only the flux of the narrow components were used. The $E(B-V)$ correction was not applied to broad line features because at the densities found in the BLR ($n_e > 10^9$ cm^{-3}) many other processes different to pure recombination should affect the flux of the permitted lines.

The intrinsic FWHM values of Hα for the galaxies studied here are listed in Table 6. These values were obtained from the subtraction, in quadrature, of the

TABLE 3

ROSAT LUMINOSITIES AND *IRAS* FLUXES FOR THE GALAXIES

Galaxy (1)	log L_X[a] (2)	12 μm (mJy) (3)	25 μm (mJy) (4)	60 μm (mJy) (5)	100 μm (mJy) (6)	α(25, 12) (7)	α(100, 60) (8)	$L_{IR}/L_\odot$ ($\times 10^{10}$) (9)
MCG −5-13-17.....	41.56[b]	224±43	570±34	1396±98	1993±159	−1.27	−0.70	0.95
CTS H34.03	...	79±18	169±17	480±43	1220±256	−1.04	−1.83	21.17
CTS B31.01.....	42.71[b]	533	700	<420	1000	−0.38	−1.70	8.72
CTS H34.06	...	<61	88±14	237±36	<873	−0.49	−2.55	1.51
Mrk 1239	42.33[b]	650±72	1141±80	1335±107	<2412	−0.77	−1.16	4.60
CTS J04.08	43.40[c]	139±39	411±40	2545±15	3704±333	−1.48	−0.73	10.24
CTS J07.02	...	<116	<120	228±48	<679	−0.05	−2.14	2.07
CTS J10.09	...	<125	<187	382±69	<810	−0.55	−1.47	1.27
CTS R12.15	...	<155	<266	784±71	1329±186	−0.74	−1.03	0.71
CTS R12.02	42.82[b]	171±32	370±81	1163±81	2222±289	−1.03	−1.27	0.89
CTS J15.22	44.34[d]	...	...	...	...	...	...	...
CTS M17.17.....	...	<74	<181	275±44	773±200	−1.22	−2.02	0.22
1H 1934−063	...	496±35	1064±64	2808±140	4754±475	−1.04	−1.03	1.30
1H 2107−097	...	130±26	350±45	270±21	<1980	−1.35	−3.93	2.55

[a] Log of *ROSAT* (0.1–2.4 keV) luminosity in units of ergs s^{-1}.
[b] Rush et al. 1996.
[c] Moran, Halpern, & Helfand 1996.
[d] Brinkmann, Siebert, & Boller 1994.

observed FWHM and that of the instrumental profile, measured from the comparison lamp lines (FWHM $\sim$ 360 km s^{-1}). It can be seen than in NLS1's the FWHM of the broad component is clearly smaller than the typical FWHM of the broad lines of normal Seyfert 1 galaxies.

Usually the broad-line flux of the permitted lines in NLS1's is comparable to the flux of the narrow component, contrary to what is observed in normal Sy1's, where nearly 90% of the flux of a given Balmer line is associated to the BLR. In column (4) of Table 6 we have listed the ratio between the narrow and broad fluxes found for Hα. Almost all NLS1's have ratios around 1, while in some normal Sy1's, it goes down to 0.04.

4.1. *Evidence of Optically Thin Gas in the BLR of Seyfert 1 Galaxies*

The absence of broad permitted lines (i.e., lines with FWHM larger than 3000 km s^{-1}) in NLS1's can be interpreted as being due to absence of gas moving at high velocity (in the line of sight) in the BLR of these objects. Osterbrock & Pogge (1985), Goodrich (1989), Stephens (1989), and Puchnariewitz et al. (1992) argue that if the BLR clouds are confined to move in a plane, the emission lines will be narrower when the line of sight is nearly aligned with the axis of that plane. Another possibility is that NLS1's have central black hole masses smaller compared to those in normal Sy1's (Ross & Fabian 1993). If the kinematics of the BLR is dominated by the central black hole, smaller masses would result in lower cloud velocities provided these clouds are located at distances similar to those in normal Sy1's.

However, Rodríguez-Pascual et al. (1997) report the detection of broad wings in the UV emission lines Lyα, He II λ1640, and C IV λ1550 of many NLS1 galaxies detected by the *IUE* at sufficiently high S/N. This finding demonstrates the existence of gas with a large velocity component in our line of sight, implying that the profiles are qualitatively similar to those found in normal Seyfert 1's. They explain the narrowness of broad optical lines as being due to the absence of a hydrogen partially ionized (HPI) zone in the high-velocity component of the BLR in NLS1's.

The above means that high-ionization lines such as He II λ1640 and C IV λ1550 would display broad components in the spectrum, while low-ionization lines (H I Balmer lines) do not. H Lyα may form in both HPI or hydrogen fully ionized zones, explaining the presence of broad components in this line. The absence of an HPI zone means that the hydrogen is optically thin to the Lyman continuum photons. It is then necessary to look for evidences of optically thin gas in the BLR of Seyfert 1 galaxies to obtain additional evidence of this scenario. This can be done by comparing the Hα and O I λ8446 emission-line profiles.

O I λ8446 can be produced by several mechanisms such as recombination, collisional excitation, continuum fluorescence, and Lyβ fluorescence (Grandi 1980). The first two mechanisms require the presence of O I λ7774 in the spectrum, while the third one requires the presence of O I λ7002 and O I λ7524. Lyβ fluorescence, on the other hand, does not require the production of O I λ7774, λ7002, and λ7524, so their absence is a good indicator of the predominance of this mechanism as the most probable means for the O I λ8446 emission. It takes advantage of the near coincidence of the energy levels of H I and O I and consists of a cascade following fluorescent absorption of Lyβ (see Fig. 3 of Grandi 1980). This mechanism requires large optical depths in Lyα ($\geq 10^7$; Elitzur & Netzer 1985) in order to allow its eventual absorption by an O I atom in the ground state and prevent the conversion of Lyβ to Lyα and Hα.

Assuming that the Hα line is produced by recombination and the BLR is composed of only optically thick clouds spread over a range of radii, with different velocities, this implies that Hα and O I λ8446 should share the same emission-line profile. Otherwise, the presence of significant population of optically thin clouds (i.e., Lyα with optical depths $\ll 10^6$), would produce Hα emission, but not O I λ8446. Thus, any profile differences between O I λ8446 and Hα could be taken as evidence for optically thin gas in the BLR (Morris & Ward 1989).

TABLE 4

OBSERVED NARROW EMISSION LINE FLUXES (in units of 10^{-15} ergs s^{-1} cm^{-2})

Galaxy	[O II] λ3727	[Ne III] λ3869	Hγ λ4341	[O III] λ4363	He II λ4686	Hβ λ4861	[O III] λ5007	He I λ5875	[Fe VII] λ6085	$E(B-V)$
CTS C16.16	6.4±0.3	3.6±0.3	1.3±0.1	2.1±0.1	...	2.2±0.1	35.7±0.3	...	...	0.36±0.06
MCG −5-13-17.....	25.1±3.0	35.8±3.1	...	12.6±1.2	5.6±0.5	11.2±0.4	234.1±13.1	3.3[a]	5.7±0.5	0.65±0.05
CTS H34.03	...	...	14.9±0.4	3.5±0.3	2.1±0.2	3.6±0.1	27.2±0.2	...	0.6[a]	1.37±0.03
CTS B31.01.....	6.2±0.9	6.5±1.0	3.9±0.1	...	14.0±0.8	42.6±0.5	74.5±0.8	10.2±0.4	...	1.02±0.01
CTS H34.06	11.7±1.4	3.3±0.4	17.9±0.6	3.5±0.1	1.0±0.4	18.7±0.5	34.2±0.9	3.3±0.2	1.2±0.2	0.21±0.05
Fairall 1146.....	20.9±1.0	...	6.4±0.9	5.8±0.9	6.6±1.0	9.0±0.4	133.1±3.0	...	...	1.02±0.04
Mrk 1239	3.0±0.3	6.3±0.3	22.6±1.0	10.5±0.5	9.6±0.6	51.5±0.5	146.9±0.5	9.5±0.6	10.3±0.9	0.52±0.03
CTS J03.19	4.0±0.6	3.0±0.5	1.8±1.0	...	1.8±0.2	3.3±0.2	24.6±1.2	2.0±0.6	...	0.56±0.06
CTS J04.08	1.0±0.2	1.1±0.2	1.1±0.1	0.5±0.1	0.7±0.1	1.9±0.2	5.1±0.5	0.6±0.1	...	0.66±0.10
CTS M02.30.....	2.3±0.1	3.6±0.2	7.0±0.4	2.7±0.1	1.0±0.2	6.9±0.2	14.4±0.6	2.6±0.1	...	0.48±0.03
CTS J07.02	35.8±3.0	6.3±0.6	7.7±0.4	4.2±0.2	3.6±0.2	30.9±0.3	198.0±2.0	4.3±0.3	...	0.68±0.01
CTS J10.09	3.9±0.7	5.7±1.3	...	5.9±0.5	2.6±0.8	3.1±0.1	37.7±0.9	4.0±0.3	3.0±0.4	0.89±0.05
CTS R12.15	...	...	3.5±0.4	0.9[a]	...	2.4±0.1	11.4±0.2	...	...	0.81±0.04
CTS R12.02	36.9±3.4	16.5±2.0	67.3±2.6	12.4±0.5	9.5±1.1	48.3±0.9	251.8±4.5	9.4±0.3	1.3±0.5	0.35±0.02
CTS J13.12	...	...	23.8±1.0	8.0±1.0	8.9±0.4	34.6±1.3	25.8±0.1	8.0±0.4	3.3±0.2	0.49±0.04
CTS J14.05	4.4±0.9	...	2.3±0.3	2.3±0.3	...	1.3±0.3	25.6±2.0	...	...	0.76±0.10
CTS J15.22	...	...	15.4±2.0	9.0±1.0	2.7±0.5	6.0±0.1	86.6±2.4	1.0±0.1	...	0.34±0.02
CTS M17.17.....	...	...	...	...	...	47.2±1.5	180.0±4.5	...	...	0.83±0.02
CTS G03.04	...	4.6±0.5	2.9±0.1	1.9±0.2	2.0±0.3	3.8±0.3	24.0±0.2	...	...	0.70±0.07
1H 1934−063	21.0±2.0	16.1±2.0	35.9±0.7	7.3±0.3	10.0±1.5	82.0±3.9	167.0±8.0	23.5±1.6	7.3±1.0	0.41±0.04
1H 2107−097	...	10.0±1.3	39.0±2.0	7.7±0.4	17.3±0.6	42.4±0.3	45.4±0.3	6.8±0.3	6.2±0.8	0.64±0.04
CTS A08.12	11.3±0.9	14.1±0.7	1.6±0.1	6.7±0.3	4.4±0.9	8.0±0.4	88.3±4.4	...	3.7±0.3	0.05±0.05
CTS F10.01.....	5.9±0.3	6.9±0.2	7.5±0.9	2.2±0.1	2.5±0.5	6.1±0.3	56.3±1.0	1.1±0.3	5.6±0.4	0.01±0.03
CTS C16.16	1.5±0.1	...	10.0±0.5	3.0±0.2	3.1±0.1	2.7±0.1	0.9±0.1	0.6[a]	...	0.36±0.06
MCG −5-13-17.....	19.0±2.1	2.1±0.2	69.7±1.0	37.3±0.5	10.0±0.5	10.9±0.5	6.2±1.6	6.9±1.5	7.3±2.5	0.65±0.05
CTS H34.03	...	...	48.9±0.5	13.3±0.1	1.7±0.1	1.1±0.1	...	...	...	1.37±0.03
CTS B31.01.....	3.2±0.2	6.5±0.4	396.3±1.2	37.8±0.1	2.7±0.1	4.0±0.2	...	...	...	1.02±0.01
CTS H34.06	3.1±0.3	1.6±0.2	72.6±0.4	17.0±0.1	5.9±0.2	5.2±0.2	1.5±0.5	2.1±0.4	1.9±0.5	0.21±0.05
Fairall 1146.....	12.3±0.7	3.4±0.9	83.2±1.0	98.1±3.0	20.4±0.7	21.5±0.7	7.8±1.0	7.1±1.5	31.6±3.0	1.02±0.04
Mrk 1239	6.1±0.3	12.4±0.6	280.4±2.5	25.3±0.1	7.4±0.3	7.6±0.3	2.5±0.1	7.1±0.3	5.0±0.7	0.52±0.03
CTS J03.19	1.6±0.3	0.6[a]	18.7±0.2	16.9±0.3	2.9±0.4	2.5±0.3	1.0±0.3	1.4±0.3	...	0.56±0.06
CTS J04.08	0.4±0.1	0.2[a]	12.2±0.2	9.3±0.9	1.4±0.3	1.4±0.3	...	...	1.0±0.2	0.66±0.10
CTS M02.30.....	1.6±0.1	...	35.9±0.2	7.7±0.1	...	...	0.9[a]	...	...	0.48±0.03
CTS J07.02	5.7±0.9	0.5[a]	198.0±2.0	27.0±0.1	3.8±0.4	3.8±0.4	9.0±2.0	...	...	0.68±0.01
CTS J10.09	2.8±0.4	...	25.0±0.8	17.3±0.1	2.1±0.1	3.4±0.1	1.2±0.2	1.9±0.3	...	0.89±0.05
CTS R12.15	1.4±0.1	2.0±0.5	17.8±0.2	10.7±0.1	2.6±0.1	2.1±0.1	...	...	4.8±0.8	0.81±0.04
CTS R12.02	8.6±0.6	1.6±0.1	217.7±0.8	123.1±0.4	26.7±0.7	25.4±0.6	4.9±0.8	...	22.6±3.2	0.35±0.02
CTS J13.12	...	5.4±0.4	181.7±1.1	11.2±1.0	1.1±0.1	1.2±0.1	...	...	...	0.49±0.04
CTS J14.05	2.4±0.4	...	9.1±0.3	9.0±0.3	5.1±0.3	3.4±0.2	...	...	...	0.76±0.10
CTS J15.22	3.5±0.8	...	26.7±0.3	9.8±0.1	1.8±0.2	3.2±0.3	...	...	...	0.34±0.02
CTS M17.17.....	48.2±1.2	...	355.6±2.0	76.2±0.8	43.8±1.2	48.3±1.2	...	...	...	0.83±0.02
CTS G03.04	1.4±0.3	1.3±0.2	24.9±0.1	18.7±0.1	2.5±0.3	1.3±0.2	1.5[a]	...	...	0.70±0.07
1H 1934−063	9.3±0.9	10.9±1.0	393.5±4.0	88.4±0.9	21.2±0.2	22.6±0.2	11.7±1.0	8.8±0.4	34.4±1.5	0.41±0.04
1H 2107−097	3.8±0.7	...	263.0±1.5	19.5±0.1	2.8±0.1	2.2±0.1	...	...	...	0.64±0.04
CTS A08.12	8.7±0.5	3.5±0.2	26.3±0.1	...	2.2±0.1	2.2±0.1	1.8±0.2	6.7±0.3	...	0.05±0.05
CTS F10.01.....	1.8±0.2	0.5[a]	17.4±0.5	9.0±0.3	3.7±0.3	3.4±0.3	...	...	...	0.01±0.03

[a] Upper limit.

In Figure 3 we plot Hα (*thick line*) and O I λ8446 (*thin line*) for the galaxies in which both profiles are observed. They have been normalized to unity and binned to velocity space. In all cases [N II] λλ6548, 6584 were removed from Hα but the narrow component of the Balmer line was kept in order to look for narrow O I λ8446 emission. The bump in the red wing of O I in 1H 1934−063 is attributed to Ca II λ8498. This emission line is part of the Ca II triplet and is produced in a region with high density and low ionization, as O I λ8446. Ca II emission is not so common, and it has been observed in other Seyfert 1's but rarely in Seyfert 2's (Persson 1988; González Delgado & Pérez 1996).

A detailed inspection to the profiles of Figure 3 allows us to conclude the following:

1. Hα and O I λ8446 have similar line profiles in all but one of the objects studied. This suggests either that optically thin material contributes a negligible amount of the Hα emission or that the optically thin material shares the same spatial distribution and velocity field as the optically thick material. Only in CTS J07.02 is there evidence for differences between the two profiles. The narrow component of O I seems narrower than Hα, and most important, its broad profile lacks the extended wings displayed by Hα. These differences can be interpreted as evidence for the presence of thin gas that prevents the O I λ8446 formation.

2. A narrow component associated with the O I λ8446 emission is observed in most of the galaxies. In Mrk 1239, 1H 1934−063, and CTS J13.12, the presence of a narrow

TABLE 5

OBSERVED BROAD EMISSION LINE FLUXES (in units of 10^{-15} ergs s^{-1} cm^{-2})

Galaxy (1)	Hγ λ4341 (2)	Hβ λ4861 (3)	He I λ5875 (4)	Hα λ6563 (5)	He I λ7065 (6)	O I λ8446 (7)	Fe II/Hβ (8)	α (9)
CTS C16.16	...	15.7±0.2	...	62.7±3.0	...	...	...	−1.62±0.10
MCG −5-13-17.....	60.6±4.0	219.5±5.0	61.8±4.0	642.0±8.0	...	...	0.32±0.05	−1.80±0.15
CTS H34.03	...	71.7±0.4	28.3±3.0	137.0±1.4	...	...	0.42±0.04	−1.06±0.07
CTS B31.01.....	55.9±2.2	134.8±2.2	19.9±1.8	1122.2±5.1	24.8±2.1	77.0±3.2	0.36±0.02	...
CTS H34.06	...	18.5±0.7	5.3±0.4	59.5±1.0	5.0±0.5	1.8[a]	0.60±0.04	−0.52±0.04
Fairall 1146.....	...	27.4±0.9	...	228.6±2.0	...	39.0±4.0	...	...
Mrk 1239	...	45.0±0.4	...	301.1±2.7	8.1±0.5	29.1±0.9	0.82±0.05	0.43±0.02
CTS J03.19	...	10.8±0.5	...	44.2±0.4	1.5±0.3	...	1.75±0.09	−0.47±0.02
CTS J04.08	...	4.1±0.08	...	15.2±0.8	...	...	0.82±0.08	−0.52±0.04
CTS M02.30.....	...	15.2±0.6	...	30.5±0.2	...	...	0.90±0.10	−0.70±0.04
CTS J07.02	67.3±3.0	112.4±1.0	21.2±1.7	471.9±4.0	15.2±1.0	23.5±1.5	...	−1.58±0.07
CTS J10.09	...	28.3±0.7	...	96.6±0.5	2.2±0.6	...	...	−0.21±0.03
CTS R12.15	...	9.9±0.4	...	29.7±0.3	...	...	...	0.40±0.02
CTS R12.02	...	114.9±3.1	24.2±1.1	299.4±1.6	7.9±1.1	26.7±3.0	0.87±0.05	−0.40±0.01
CTS J13.12	...	36.7±1.4	...	85.6±0.5	5.9±0.2	8.7±0.5	0.57±0.06	−0.74±0.05
CTS J14.05	...	19.7±2.0	...	155.3±4.7	...	...	...	...
CTS J15.22	...	73.3±2.1	20.2±2.0	263.8±3.0	...	...	0.26±0.03	−0.46±0.02
CTS M17.17.....	...	238.9±6.0	...	892.3±9.0	...	...	...	0.1±0.01
CTS G03.04	34.4±0.7	107.8±1.0	34.0±4.0	249.2±1.2	1.0[a]	18.0±0.4	...	−0.83±0.04
1H 1934−063	...	82.2±3.9	...	256.3±2.6	21.0±2.0	59.3±4.0	0.89±0.06	−0.96±0.05
1H 2107−097	...	89.0±0.5	32.0±1.5	322.4±2.0	5.6±0.2	16.1±0.8	0.55±0.05	−0.35±0.01
CTS A08.12	26.7±0.1	91.9±4.5	17.2±0.8	509.5±2.5	2.0±0.1	...	...	−0.38±0.03
CTS F10.01.....	45.9±5.0	153.5±4.0	21.0±0.1	720.0±7.2	...	...	0.87±0.09	−0.90±0.04

[a] Upper limit.

TABLE 6

FWHM OF Hα (in km s^{-1}).

GALAXY (1)	Hα FWHM Narrow (2)	Hα FWHM Broad (3)	$F(H\alpha_n/H\alpha_b)$ (4)
CTS C16.16	472	7300	0.14
MCG −5-13-17.....	352	4610	0.05
CTS H34.03	583	3330	0.05
CTS B31.01.....	1035	2772[a]	0.32
CTS H34.06	360	1918	1.01
Fairall 1146.....	687	3790	0.33
Mrk 1239	490	2375	1.14
CTS J03.19	360	1735	0.30
CTS J04.08	413	1870	1.67
CTS M02.30.....	890	3470	0.45
CTS J07.02	890	2830	0.27
CTS J10.09	360	2920	0.11
CTS R12.15	740	3290	0.24
CTS R12.02	635	2375	0.42
CTS J13.12	636	2375	0.95
CTS J14.05	413	4295	0.07
CTS J15.22	472	3790	0.08
CTS M17.17.....	938	4385	0.20
CTS G03.04	687	3190	0.04
1H 1934−063	740	2650	1.00
1H 2107−097	1370	3835	0.48
CTS A08.12	530	4570	0.09
CTS F10.01.....	583	5205	0.04

[a] There is a very broad component with FWHM of 11,000 km s^{-1}, clearly present in Hα but not observed in Hβ.

component of O I is not evident, but it is certainly present given that the Hα and O I λ8446 profiles are very similar and the narrow component of the former line was not removed. Only in 1H 2107−097 was no evidence of narrow a component for the O I found. Grandi (1980), Morris & Ward (1989), and González Delgado & Pérez (1996) had associated the O I λ8446 emission with a purely broad-line phenomenon, and no narrow emission from this line was reported by them. In fact, in the profile comparison of Morris & Ward (1989) no narrow profile in the O I λ8446 line is seen, except in Mrk 1239, but the authors did not mention it explicitly.

The above results point out the presence of large optical depths in Lyα ($\geq 10^7$) in the BLR of 1H 2107−097 and in both in the NLR and BLR of the remaining galaxies of Figure 3.

Based on the similarity of the line profiles of Hα and O I for the NLS1's studied here, we can also conclude that no evidence of thin gas emission is found in the BLR of these objects. This result goes against the hypothesis of the lack of an HPI zone in the high-velocity gas to explain the absence of broad lines in our NLS1's. Another mechanism should be operating in these objects that prevents the broad components of the Balmer lines from being observed.

5. ANALYSIS OF THE NLR OF NLS1 AND NORMAL SY1 GALAXIES

The narrow line fluxes of Table 4 were corrected for reddening using the $E(B-V)$ values listed in the last column of that table. In this correction, the Cardelli, Clayton, &

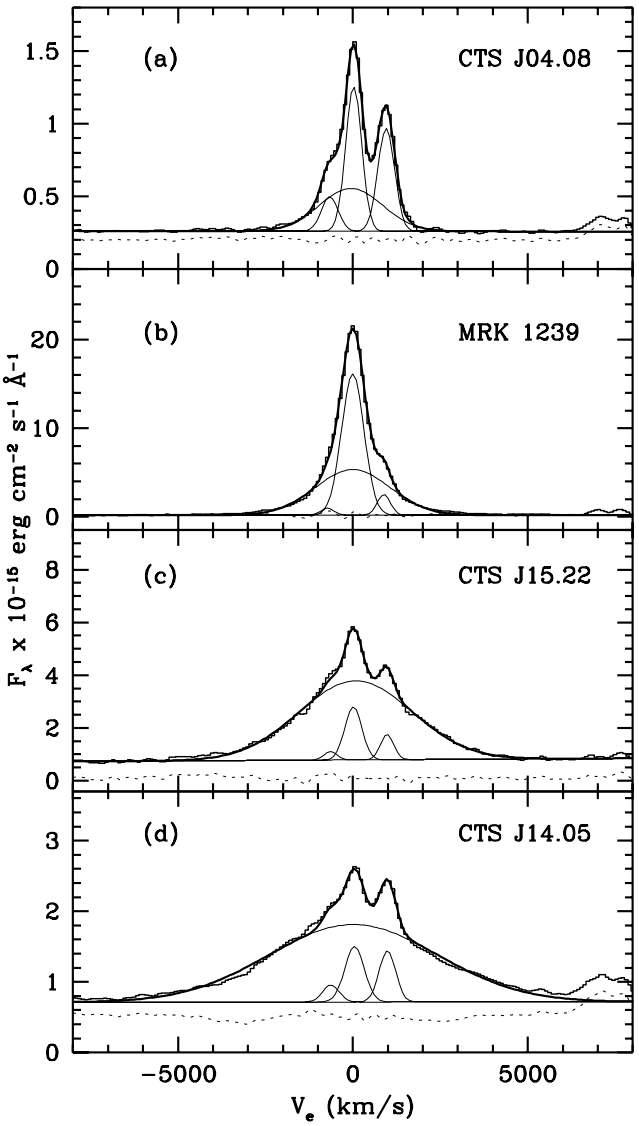

FIG. 2.—Deblending of the Hα + [N II] λλ6548, 6584] lines in the NLS1 galaxies CTS J04.08 (*a*) and Mrk 1239 (*b*) and normal Seyfert 1 galaxies CTS J15.22 (*c*) and CTS J14.05 (*d*) showing the decomposition into narrow and broad profiles (*thin lines*) using the Gaussian representation discussed in the text. The thick line shows the total fit, and the dotted line, the residuals of the fit. The feature longward of 6000 km s^{-1} are due to [S II] λλ6717, 6731.

Mathis (1989) extinction function was used. The reddening-corrected fluxes will be employed throughout this section to compare the emission properties of the narrow-line regions of normal Sy1 and NLS1 galaxies.

We have to stress here that given the good S/N spectra of the NLS1's, it was possible to isolate the narrow component of the Hα line from the broad one in these objects (see § 4). We associate the narrow profiles of the permitted lines with emission from the NLR because they have essentially the same width as that of the forbidden lines.

Figure 4 shows the $E(B-V)$ plotted against the FWHM of the broad component of Hα for our data. Filled triangles represent normal Sy1 galaxies and full circles NLS1 galaxies. Error bars are at 3 σ significative level. According to this figure, NLS1's tend to have lower values of reddening than normal Sy1's. We have found, on average, an $E(B-V)$ value of 0.46 mag for the former and 0.66 mag for the latter. It is not possible to say if the continuum is affected by the same amount of reddening as the emission lines, but the fact of NLS1's having flatter optical spectral index than normal Sy1 galaxies suggests that their optical continuum may suffer of larger extinction.

It is also interesting to see how the featureless optical continuum at 4800 Å correlates with the broad Hα luminosity, as is shown in Figure 5. We found that our galaxies follow the well-established correlation between line and continuum luminosity, determined by Yee (1980) and Shuder (1981), suggesting that the predominant mechanism of gas excitation in both NLS1 and normal Sy1 galaxies is photoionization.

5.1. *Excitation of NLS1's and Normal Sy1's: What Does the Traditional Diagnostic Diagram Say*

In Figure 6 we have used the diagnostic diagram [O III] λ5007/Hβ versus [N II] λ6584/Hα of Veilleux & Osterbrock (1987) to look for differences in the degree of excitation of the NLRs of the galaxies. It can be seen that both NLS1's and normal Sy1's are scattered across the diagram. Most "normal" Seyfert 1's (*filled triangles*) show line ratios typical of AGNs, while some others are located in transition zones normally occupied by starburst galaxies and H II regions. NLS1 galaxies (*filled circles*) are mainly located in the lower left-hand part of the figure, meaning that they are less excited than normal Sy1's. Stephens (1989) presented similar results for her sample of Seyfert 1 objects, but she employed the total flux of Hα and Hβ in the line ratios, causing the points to segregate naturally from the AGN region and fall in the lower left-hand corner of the figure. Here we show that even considering narrow-line fluxes in the permitted lines, there is a large spread of values for the line ratios involved and thus that diagram cannot be used to distinguish Seyfert 1 galaxies from other AGNs.

According to the unification model (Antonucci & Miller 1985), the NLRs of Sy1 and Sy2 galaxies should have similar degrees of excitation. However, Figure 6 tells us that this may not be true. We find that the NLRs of Sy1 galaxies have line ratios that range from those of a typical H II region up to those very similar to those of Seyfert 2's.

5.2. *Other Line-Ratio Plots*

Figures 7*a*–7*f* show [O II] λ3727/[O III] λ5007, He II λ4686/Hβ, [Fe X] λ6374/Hα, [O III] λ4363/[O III] λ5007, [S II] λ6717 + λ 6731/Hα, and [O I] λ6300/Hα plotted against [O III] λ5007/Hβ.

An inspection of the above plots allows us to say that NLS1 and normal Seyfert 1 galaxies appear to merge continuously with each other in most of the line ratios involved. This property is not restricted to the optical region. Boller et al. (1996) had also found the same result in their plot of the *ROSAT* 0.1–2.4 keV photon index versus the FWHM of Hβ. Also, Goodrich (1989) argued that the differences between NLS1 and normal Sy1 galaxies really represent a continuum of properties.

However, we found that in the diagrams involving low ionization lines, normal Seyfert 1's seem to cover a wider range of values than NLS1's. For example, in Figure 7*e*, no NLS1 galaxy has [S II] λ6717 + λ6731/Hα larger than 0.3, while normal Seyfert 1 galaxies have values up to 0.9. Also, [O I] λ6300/Hα (Fig. 7*f*) is no larger than 0.1 in NLS1's, while in normal Seyfert 1's it goes up to 0.35.

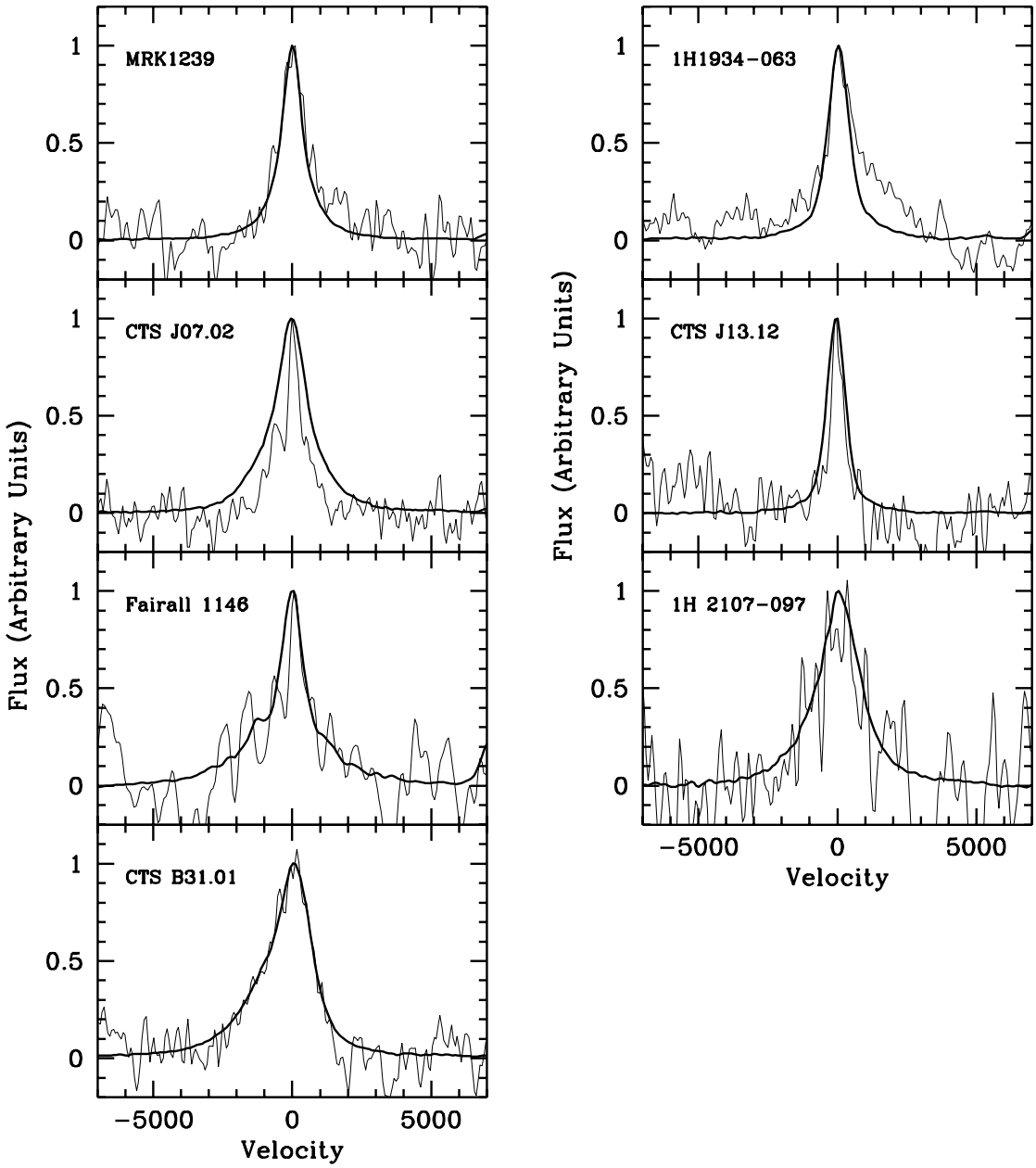

FIG. 3.—Comparison of the Hα (*thick line*) and O I λ 8446 (*thin line*) emission-line profiles in velocity space. The bump in the red wing of 1H 1934−063 is due to Ca II λ8498 emission.

When high-ionization lines are analyzed, as for example [Fe X] λ6374/Hα versus [O III] λ5007/Hβ (Fig. 7*c*), we see that both groups of galaxies share the same range of values. Another good example is the ratio [O III] λ4363/[O III] λ5007, which maps the temperature in the [O III] zone. According to Figure 7*d*, NLS1's and normal Sy1's show no difference in temperature in the central parts of their NLRs.

In order to see if the above trends are observed in other NLS1s, we have plotted with crosses in Figures 7*a*–7*f* data for Mrk 42, Mrk 359, Mrk 493, Mrk 766, Mrk 783, and Mrk 1126, taken from Osterbrock & Pogge (1985), and NCG 4253, taken from González Delgado & Pérez (1996). It can be seen that these points also follow the same behavior as our NLS1s, giving additional support to our results.

Are [O I] λ6300/Hα, [S II] λ6717+λ6731/Hα, and [O II] λ3727]/Hβ intrinsically low in NLS1's, or are we seeing them as low because the Balmer emission lines are stronger in these objects? In order to answer this question we have plotted in Figures 8*a*–8*h* several narrow-line luminosities versus the FWHM of the broad Hα line for the galaxies of our sample and those taken from the literature.

Figure 8 favors the interpretation that low-ionization lines are intrinsically weak in NLS1s. In Figure 8*a*, we see that both groups of galaxies have essentially the same values of Hα luminosity, meaning that it is not a high Hα or Hβ in NLS1's that makes the above ratios smaller. Figures 8*c* and 8*f* separate NLS1's from normal Sy1's in the luminosity axis. In average, the [O I] λ6300 and [O II] λ3727 luminosity in NLS1's is smaller than in normal Sy1's. Other low-ionization lines such as [N II] λ6584 and [S II] λλ6717, 6731 (Figs. 8*d* and 8*h*, respectively), show the same behavior as [O I] λ6300 and [O II] λ3727. The same can be said for [O III] λ5007 (Fig. 8*b*), although this result was expected given that NLS1's are characterized by a low [O III] λ5007/

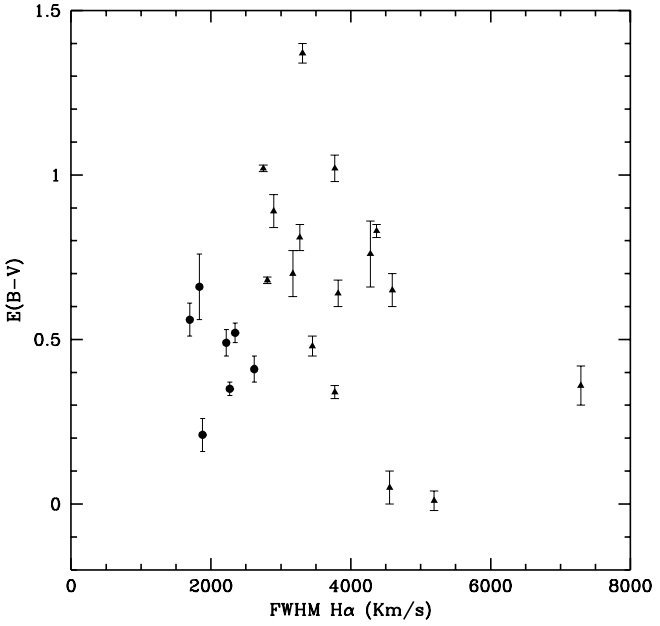

FIG. 4.—Plot of $E(B-V)$ vs. the FWHM (in km s^{-1}) of the broad component of Hα. Filled triangles represent normal Sy1 galaxies, and filled circles, NLS1 galaxies. The error bars are 3 σ significative.

Hβ ratio. [O III] λ4363 has the opposite behavior, being stronger in NLS1's. For this reason, the [O III] temperatures in NLS1,s are nearly the same as those in normal Sy1's. High-ionization lines such as [Fe X] λ6374 (Fig. 8*e*) do not differentiate between the two groups of galaxies.

5.3. *Physical Conditions in the NLR*

In this section we use the density indicator [S II] λ6717/[S II] λ6731 and the temperature indicators [O II] λ3727/[O II] λ7324 and [O III] λ4363/[O III] λ5007 to map the physical conditions inside the NLR of the Seyfert 1 galaxies of our sample.

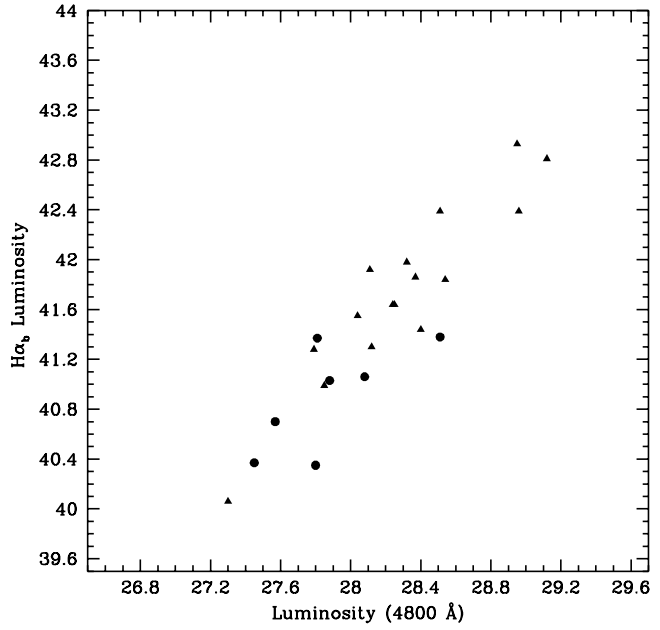

FIG. 5.—Logarithm of the broad Hα luminosity (in units of ergs s^{-1}) plotted against the logarithm of the continuum luminosity at 4800 Å, in units of ergs s^{-1} Hz^{-1}. Symbols are the same as those of Fig. 4, and their sizes are, in all cases, representative of the error bar at 3 σ significative level.

Under normal photoionization conditions, [O II] λ3727 and [S II] λλ6717, 6731 are emitted in the same region because they have similar critical densities and ionization potentials. If these lines, along with [O II] λ7324, are present in a given spectrum, it is possible to determine iteratively, without ambiguity, the density and temperature of the region in which they are formed. The procedure is as follows. An initial guess for the density is obtained using the [S II] ratio, assuming a temperature of, for example, 10^4 K. This density is then used to derive $T_{[O\,II]}$. If it differs from the initial value of T by more than 5%, a new n_e is derived using the $T_{[O\,II]}$ obtained in the previous step. The iteration continues until a convergence is reached, that is, until two consecutive values of n_e and $T_{[O\,II]}$ are very similar.

The above procedure were applied to 10 galaxies, and the results are listed in Table 7. In this calculation we used the task *nebular* of the STSDAS package of IRAF. Errors in the $T_{[O\,II]}$ temperature are about 3000 K. Convergence was possible in four objects (CTS C16.16, MCG −5-13-17, Fairall 1146, and CTS J10.09). Average values for density and temperature are around 10^3 cm^{-3} and 12,000 K, respectively.

In four NLS1 galaxies (CTS H34.06, Mrk 1239, CTS J03.19, and 1H 1934−063) and one normal Sy1 galaxy (CTS A08.12), a first estimate of the density n_e assuming a temperature of 10^4 K gave no solution for $T_{[O\,II]}$. In order to obtain $T_{[O\,II]}$ values similar to those found in the first four galaxies (that is, $T_{[O\,II]} \sim 12{,}000$ K), it was necessary to assume higher densities ($n_e \sim 5 \times 10^3$ cm^{-3} to 3×10^4 cm^{-3}) than those derived from the [S II] λ6717/λ6731 ratio. This result suggests that in these objects, the [S II] and [O II] lines are not formed in the same region.

Table 7 also lists $T_{[O\,III]}$, derived assuming electron densities of 10^5 cm^{-3} (col. [4]) and 10^6 cm^{-3} (col. [5]). Errors associated with $T_{[O\,III]}$ are around 4000 K. In most cases, densities lower than 10^5 cm^{-3} give temperatures larger than 6×10^4 K, which are unlikely to exist in the NLR via photoionization by a central source.

It is possible to use $T_{[O\,III]}$ to constrain n_e in the [O III] zone using the fact that this temperature is not expected to be lower than $T_{[O\,II]}$. For example, in CTS C16.16, n_e is more likely to be around 10^5 cm^{-3} since larger densities will produce a $T_{[O\,III]}$ lower than that of $T_{[O\,II]}$. This density is in very good agreement with the results of Rodríguez-Ardila et. al. (1996), who found a density of 10^5 cm^{-3} from photoionization modeling of that object. Here, we confirm their predictions using another approach. The same idea can be applied to MCG −5-13-17, Fairall 1146, and CTS J10.09, where the n_e in the [O III] zone should be around 10^5 cm^{-3}. NLS1 galaxies as well as other normal Sy1's such as CTS M02.30, CTS J15.22 and 1H 2107−097 should have n_e in the [O III] region $\geq 10^6$ cm^{-3}. Lower values of density would raise $T_{[O\,III]}$ to extremely large values.

These results are in very good agreement with Figures 7*d* and 8*b*, where galaxies with large λ4363/λ5007 ratios have low λ5007/Hβ ratios and intrinsic low λ5007 luminosity. We have found that in these objects the density in the [O III] zone should be around 10^6 cm^{-3}. At this density, collisional de-excitation of [O III] λ5007 is important, making this line appear quenched relative to [O III] λ4363 and Hβ.

Summarizing this section, our data suggest that a large range of densities, covering at least 4 orders of magnitude (10^2 cm^{-3} to 10^6 cm^{-3}), must exist in the NLRs of Seyfert 1 galaxies. In normal Sy1's, the [S II] and [O II] regions are

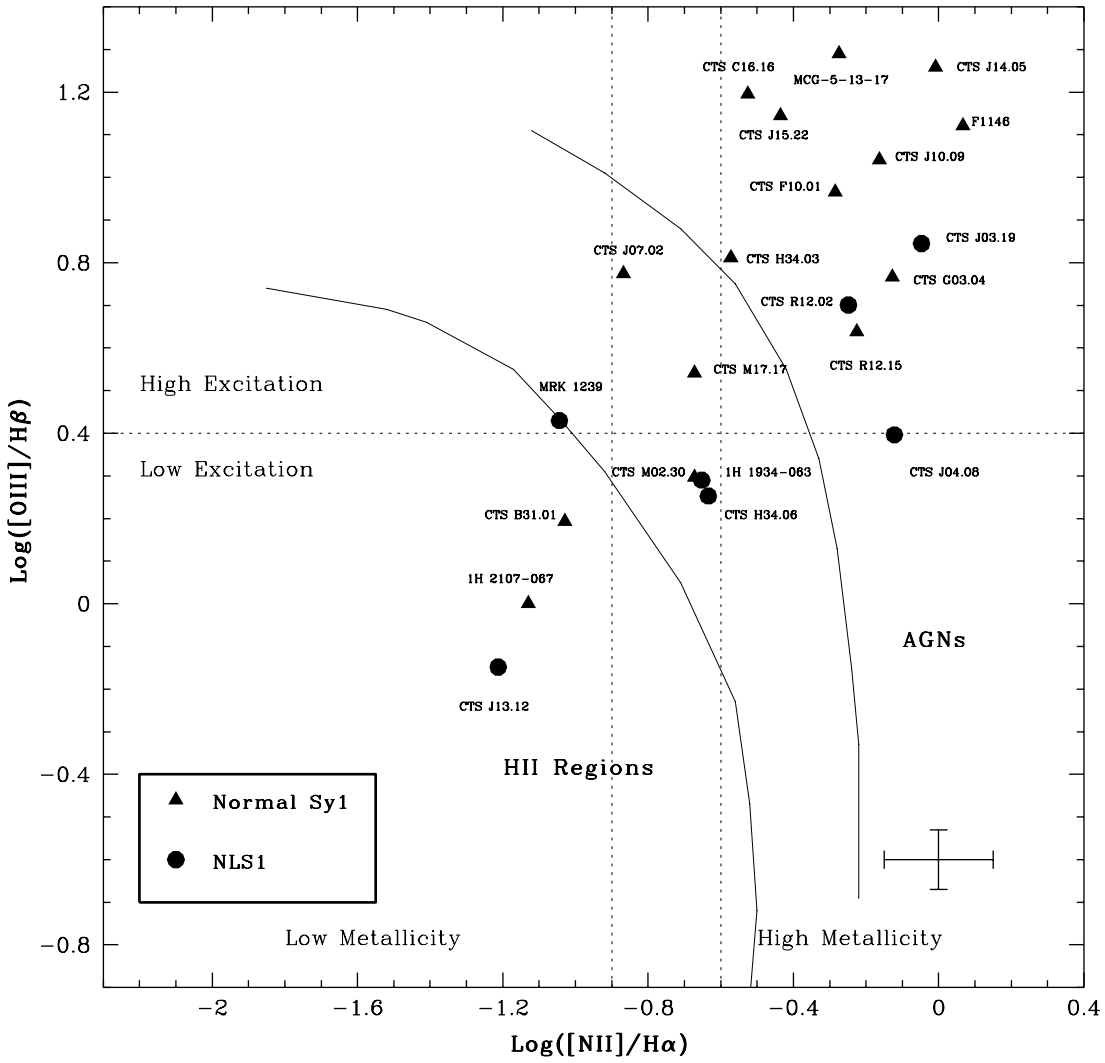

FIG. 6.—[O III] λ5007/Hβ vs. [N II] λ6584/Hα for the galaxies of our sample. Note that most NLS1 galaxies and some normal Sy1's are out of the region usually occupied by AGNs. Hα and Hβ correspond to the fluxes of the narrow components only.

overlapping and can be characterized by densities around 10^3 cm^{-3} and temperatures near 12,000 K. In NLS1's, these two regions seem to be separated, with typical densities near 5×10^2 cm^{-3} in the former and 10^4 cm^{-3} in the latter. Deep into the NLR, where most of the [O III] emission and high-ionization lines are formed, densities larger than 10^5 cm^{-3} and temperatures as high as 30,000 K can be found both in normal and NLS1 galaxies.

Among potential sources of uncertainties that can affect some of the results of the above sections we can list the following:

1. An inadequate subtraction of the stellar population that can lead to an overestimate of the flux in the λ4363 line, giving a larger $T_{[O\,III]}$.
2. Low S/N spectra that can lead to an inadequate deblending of the Hγ + [O III] λ4363, affecting the flux of the latter line.
3. A bad $E(B-V)$ correction giving larger $T_{[O\,II]}$ temperatures.
4. The presence of Fe II residual, even after subtraction of this continuum, since it interferes with the measurements of the [O III] λ5007 and [O III] λ4363 line fluxes.

However, we estimate that our data are not seriously affected by the above factors since a clean subtraction of the continuum components (see § 3) and a good separation of strong blended lines (see § 4) were carried out in most of the galaxies of our sample.

It is important to note that the above description is very simple and by no means describes the full range of physical conditions inside the NLRs of Seyfert 1 galaxies. Additional density- or temperature-sensitive ratios involving ions of higher ionization potential and/or critical densities are necessary not only to confirm our results but also to map whole range of temperatures and densities that seems to be present across the NLR.

6. SUMMARY AND CONCLUSIONS

We have carried out a spectroscopic study in the optical, near-IR, and IR bands of a sample composed of seven narrow-line Seyfert 1 and 16 normal Seyfert 1 galaxies in order to study the continuum and line emission properties of these objects . The following are the main results.

1. We have found from the optical continuum distribution that in CTS M17.17, CTS R12.15, and MCG −5-13-

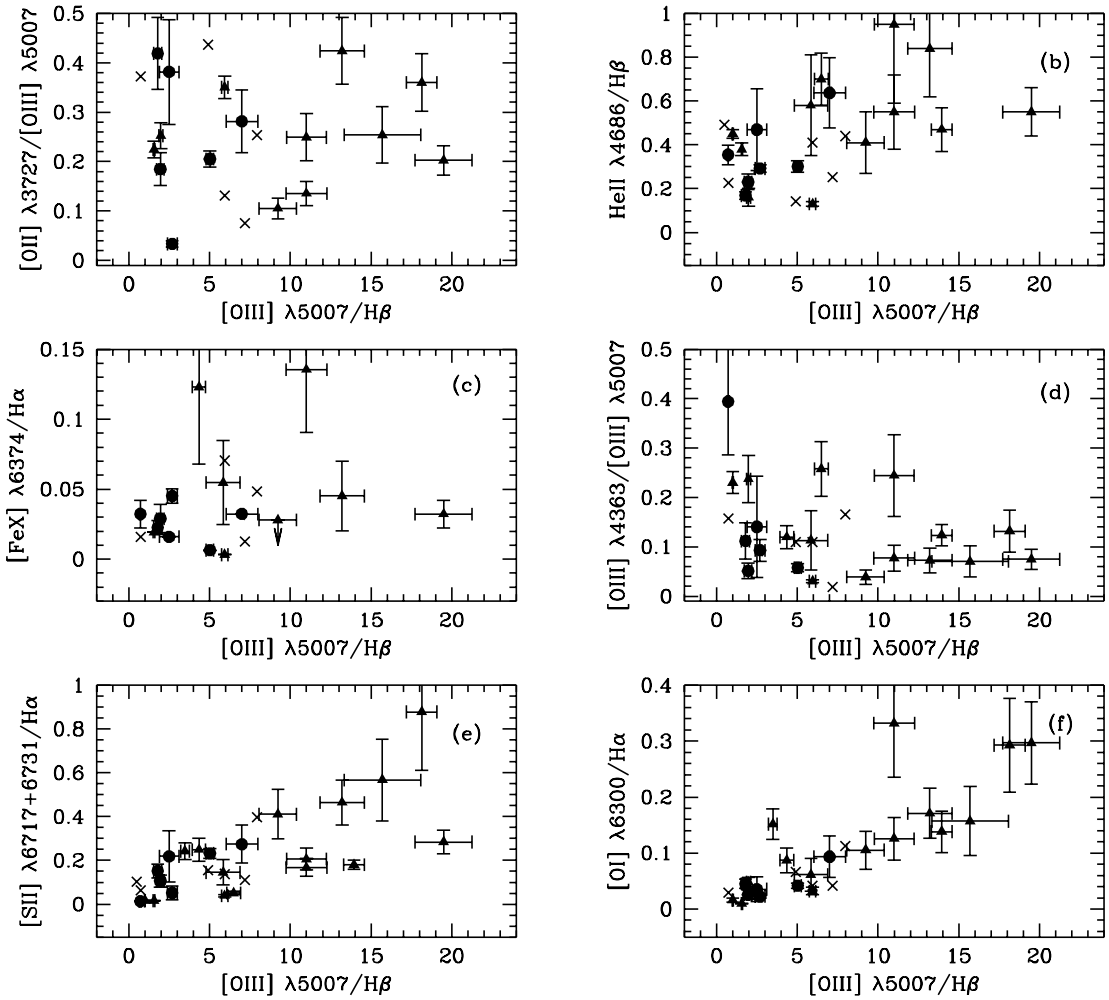

FIG. 7.—Several narrow emission line ratios plotted against [O III] λ5007/Hβ. Symbols are the same as Fig. 6. Crosses represent NLS1s taken from the literature (see text for more details). The error bars are 3 σ significative.

17, the stellar population contributes 60%, 70%, and 44%, respectively, of the continuum at 5870 Å. For the remaining galaxies, the stellar population contribution to the total continuum is negligible. Differences in the power-law index α of the nonthermal continuum component are found between NLS1 and normal Sy1 galaxies, the latter objects usually presenting steeper slopes. Another important component of the observed continuum, mainly in NLS1's, is the Fe II emission. Its contribution, quantified by the Fe II/Hβ ratio, is higher in NLS1's (0.92) than in normal Sy1's (0.53)

2. In the *IRAS* band, NLS1's and normal Sy1's have very similar behavior. The IR colors of our sample can be explained as a result of dust heated directly by the AGN source with some fraction of emission from cool dust ($0.2 \leq \beta \leq 0.6$) with evaporation temperature of $T_{ev} = 1500$ K. The only exception is 1H 2107−097, which shows $\alpha(100, 60) = -3.9$, very reddish for Seyfert 1 objects.

3. We have searched for evidence of thin gas emission in order to explain the narrowness of the broad permitted lines in NLS1's. This can be done by looking for differences between the line profiles of Hα and O I λ8448. Our results show that these two lines are rather similar except in CTS J07.02, a normal Sy1 galaxy. In addition, we find a narrow component associated with the O I λ8446 emission in most of the galaxies in which this line is present. This result suggests that the O I λ8448 is not a purely broad-line phenomenon, as was previously considered.

4. From the diagnostic diagram [O III] λ5007/Hβ versus [N II] λ6584/Hα, we observed that Seyfert 1 galaxies show a large range of excitation, varying from that typical of AGNs to those usually observed by H II regions and starburst galaxies. NLS1's have a larger tendency to occupy the regions of the least excited objects.

5. The NLRs of narrow-line and normal Sy1 galaxies show important differences. Low-ionization lines such as [O I] λ6300, [S II] λ6717+λ 6731, and [O II] λ3727 are intrinsically less luminous in the former than in the latter. When high-ionization lines are analyzed, for example [Fe X] λ6374, we see that both groups of galaxies are mixed and distributed uniformly. This is also true for Hα. We do not find differences in temperature for the [O III] zone in NLS1's and normal Sy1's.

6. Our data suggest that a large range of densities, covering at least 4 orders of magnitude (10^2 cm^{-3} to 10^6 cm^{-3}), must exist in the NLRs of Seyfert 1 galaxies. In Sy1's, the [S II] and [O II] regions are overlapping and can be characterized by densities around 10^3 cm^{-3} and temperatures near 12,000 K. In NLS1's, these two regions seems to be

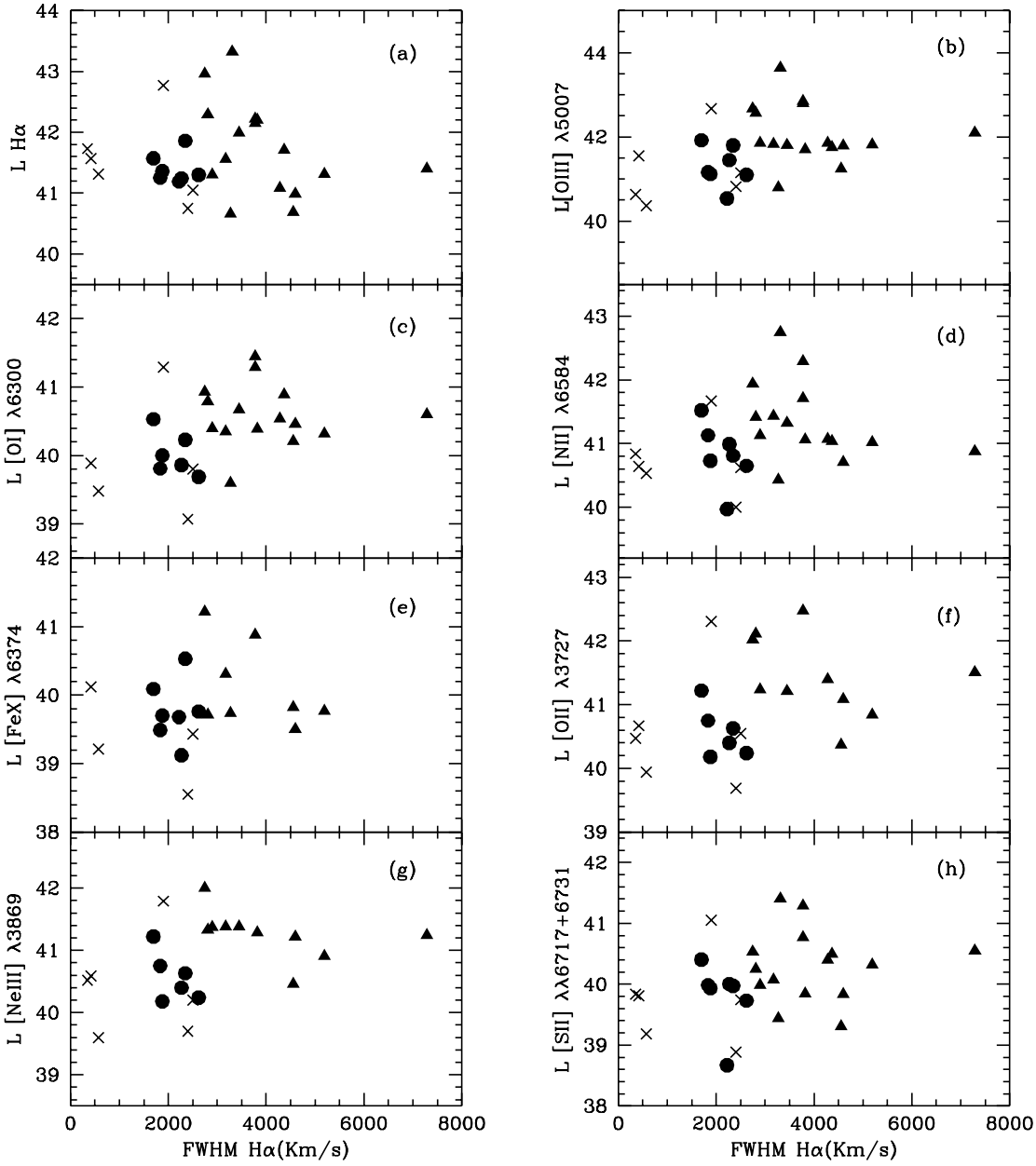

FIG. 8.—Log of the luminosity (in ergs s^{-1}) of several narrow emission lines vs. the FWHM (in km s^{-1}) of the broad component of Hα. Symbols are the same as Fig. 6. The error bar is in all cases smaller than the size of the points.

TABLE 7

PHYSICAL QUANTITIES FOR THE NLR OF THE GALAXY SAMPLE

GALAXY (1)	n_e (cm^{-3}) (2)	$T_{[O\ II]}$ (K) (3)	$T_{[O\ III]}$ (K) $n_e = 10^5\ cm^{-3}$ (4)	$T_{[O\ III]}$ (K) $n_e = 10^6\ cm^{-3}$ (5)
CTS C16.16	320	14,000	28,400	12,900
MCG −5-13-17.....	1000	14,800	31,000	13,300
CTS H34.03	10[a]	...	>60,000	37,000
CTS B31.01.....	2370	...	...	...
CTS H34.06	350[b]	12,500[c]	47,200	15,800
Fairall 1146.....	760	10,300	33,100	13,800
Mrk 1239	600[b]	14,300[c]	41,700	15,100
CTS J03.19	270[b]	12,800[c]	...	...
CTS J04.08	420	...	...	...
CTS M02.30.....	...	...	>60,000	32,100
CTS J07.02	600	...	16,200	9500
CTS J10.09	3070	9500	>60,000	33,700
CTS R12.15	170	...	>60,000	17,000
CTS R12.02	450	...	21,400	11,200
CTS J13.12	600	...	>60,000	>60,000
CTS J14.05	10[a]	...	>60,000	18,100
CTS J15.22	5300	...	>60,000	17,300
CTS M17.17.....	790	...	...	...
CTS G03.04	10[a]	...	53,700	16,400
1H 1934−063	740[b]	12,500[c]	21,500	11,300
1H 2107−097	10[a]	...	>60,000	30,700
CTS A08.12	600[b]	13,200[c]	31,100	13,500
CTS F10.01.....	400	...	18,200	10,300

[a] Lower limit.

[b] It was assumed a temperature of 10^4 K given that no solution was found for $T_{[O\ II]}$ for the first guess in density.

[c] The following densities were used in deriving T: CTS H34.06 = 3.5×10^3 cm^{-3}, Mrk 1239 = 3.2×10^4 cm^{-3}, CTS J03.19 = 3×10^3 cm^{-3}, 1H 1934 − 063 = 7×10^3 cm^{-3}, CTS A08.12 = 2.5×10^4 cm^{-3}.

separated and characterized by different densities. Deep into the NLR, where most of the [O III] emission and high-ionization lines are formed, densities larger than 10^5 cm^{-3} and temperatures as high as 30,000 K are found in both groups of objects. The low [O III] λ5007/Hβ found in most NLS1 and some normal Sy1's is most probably due to collisional de-excitation of [O III] λ5007.

A. R. A. wishes to thank Cláudia Winge for very useful comments and suggestions and the staff of CASLEO Observatory for their hospitality and technical support during the observing runs. We thank the anonymous referee for useful comments that helped to improve the quality of this paper. This work has been partially supported by the Brazilian Research Council (CNPq) to A. R. A. This research has made use of the NASA/IPAC extragalactic data base which is operated by the Jet Propulsion Laboratory, Caltech.

REFERENCES

Antonucci, R. R. J., & Miller, J. S. 1985, ApJ, 297, 621
Bica, E. 1988, A&A, 195, 76
Boller, Th., Brandt, W. N., & Fink, H. 1996, A&A, 305, 53
Bonatto, C. J., & Pastoriza, M. G. 1997, ApJ, 486, 132 (BP97)
Brinkmann, W., Siebert, J., & Boller, Th. 1994, A&A, 281, 355
Cardelli, J. A., Clayton, G. C., & Mathis, J. S. 1989, ApJ, 345, 245
Elitzur, M., & Netzer, H. 1985, ApJ, 291, 464
González Delgado, R. M., & Pérez, E. 1996, MNRAS, 278, 737
Goodrich, R. W. 1989, ApJ, 342, 224
Grandi, S. A. 1980, ApJ, 238, 17
Joly, M. 1991, A&A, 242, 49
Maza, J., Ruiz, M. T., González, L. E., & Wischnjewsky, M. 1989, ApJS, 69, 349
———. 1992, Rev. Mexicana Astron. Astrofis., 24, 147
Maza, J., Ruiz, M. T., González, L. E., Wischnjewsky, M., & Antezana, R. 1994, Rev. Mexicana Astron. Astrofis., 28, 187
Moran, E. C., Halpern, J. P., & Helfand, D. J. 1996, A&AS, 106, 341
Morris, S. L., & Ward, M. J. 1989, ApJ, 340, 713
Osterbrock, D. E., & Pogge, R. W. 1985, ApJ, 297, 166
Persson, S. E. 1988, ApJ, 330, 751
Puchnariewitz, E. M., Mason, K. O., Córdova, F. A., Kartjie, J., Branduardi-Raymont, G., Mittaz, J. P. D., Murdin, P. G., & Allington-Smith, J. 1992, MNRAS, 256, 589
Rodríguez-Ardila, A., Pastoriza, M. G., Bica, E., & Maza, J. 1996, ApJ, 463, 522
Rodríguez-Ardila, A., Pastoriza, M. G., & Maza, J. 1998, ApJ, 494, 202
Rodríguez-Pascual, P. M., Mas-Hesse, J. M., & Santos-Lleó, M. 1997, A&A, 327, 72
Ross, R. R., & Fabian, A. C. 1993, MNRAS, 261, 64
Rush, B., Malkan, M. A., Fink, H. H., & Voges, W. 1996, ApJ, 471, 190
Shuder, J. M. 1981, ApJ, 244, 12
Stephens, S. A. 1989, AJ, 97, 10
Stone, R. P. S., & Baldwin, J. A. 1983, MNRAS, 204, 347
Veilleux, S., & Osterbrock, D. 1987, ApJS, 63, 295
Walterbos, R. A. M., & Greenwalt, B. 1996, ApJ, 460, 696
Yee, H. K. C. 1980, ApJ, 241, 894